Nano Energy 72 (2020) 104706

Contents lists available at ScienceDirect

Nano Energy

journal homepage: http://www.elsevier.com/locate/nanoen

Full paper

Hierarchically structured PVDF/ZnO core-shell nanofibers for self-powered physiological monitoring electronics

Tao Yang [a], Hong Pan [a], Guo Tian [a], Binbin Zhang [a], Da Xiong [a], Yuyu Gao [a], Cheng Yan [a], Xiang Chu [a], Ningjun Chen [a], Shen Zhong [a], Lei Zhang [a], Weili Deng [a,**], Weiqing Yang [a,b,*]

[a] Key Laboratory of Advanced Technologies of Materials (Ministry of Education), School of Materials Science and Engineering, Southwest Jiaotong University, Chengdu, 610031, PR China

[b] State Key Laboratory of Traction Power, Southwest Jiaotong University, Chengdu, 610031, PR China

A R T I C L E I N F O

Keywords:
Physiological monitoring electronics
Hierarchical PVDF/ZnO nanofibers
Piezoelectric sensor
Gas permeability
Wearable electronics

A B S T R A C T

Piezoelectric-based wearable electronics promise potential applications in human physiological monitoring for disease prediction, diagnose and rehabilitation. Still, it is a big challenge to fulfill excellent compatibility and precisely monitoring of the complexly subtle physiological signals simultaneously. Here, we prepared a three-dimensional hierarchically interlocked PVDF/ZnO nanofiber-based piezoelectric sensor through epitaxial growing ZnO nano rods (NRs) on the surface of electrospun PVDF nanofibers, which enables the fiber-based physiological monitoring electronics (PME) of well flexibility and high gas permeability. Due to synergistic piezoelectric effect of the effectively deformed interlocked ZnO NRs and the uniformly orientated PVDF nanofibers with high electroactive phase, the sensitivities of PME in both pressing and bending modes have been greatly improved 6 times and 41 times than that of pure PVDF nanofibers respectively. On this basis, the designed PME can precisely detect the complexly subtle physiological signals of respiration, wrist pulse and muscle behavior. Moreover, a sensitive gait recognition system was successfully developed based on PME arrays. Therefore, this proposed fiber-based device provides an alternative strategy to monitor the human subtle physiological signals and demonstrates promising potential in the expanded application of healthcare and clinical diagnosis.

1. Introduction

Real-timely monitoring human physiological signals such as respiration, wrist pulse, muscle behavior, are of great significance for disease diagnose, therapy, rehabilitation and healthy assessment [1–4]. These human physiological signals are characterized by low frequency and tiny amplitude, so it is a huge challenge to precisely detect these signals [5–9]. With the development of nanomaterials and nanotechnology, it appears feasibility for human physiological monitoring through wearable electronics [10–16].

In this regard, wearable electronics based on piezoresistive [17,18], capacitive [19], piezoelectric [20] and triboelectric [21,22] effects have attracted extensive attentions due to their interface friendliness and versatility [23–26]. Among different working mechanisms, the piezoelectric sensors have outstanding advantages of fast response and self-powered characteristics, which displayed extensive promise in wearable electronics [27]. While the piezoelectric composite material, compromising the electric performance of inorganic ceramic and the flexibility of polymer, i.e. PVDF/$BaTiO_3$ [28], PVDF/PZT [29], and ZnO/cellulose [30] is one kind of the desired material for flexible piezoelectric sensors [31,32]. And extensive studies have focused on micro/nanostructured design of piezoelectric composite materials, such as porous films [33], nanopillar arrays [34], trigonal line-shaped and pyramid-shaped films [35], aiming to obtain well electrical performance and flexibility simultaneously [36]. Unfortunately, most of piezoelectric films still suffer from low deformation [37], bad gas permeability [28] and weak damage tolerance [38] resulting in poor suitability and compatibility, which limits their further applications. Hence, an efficient scheme is highly desired to achieve perfect overall performance in one device for physiological signals monitoring.

* Corresponding author. Key Laboratory of Advanced Technologies of Materials (Ministry of Education), School of Materials Science and Engineering, Southwest Jiaotong University, Chengdu, 610031, PR China.

** Corresponding author.

E-mail addresses: weili1812@swjtu.edu.cn (W. Deng), wqyang@swjtu.edu.cn (W. Yang).

https://doi.org/10.1016/j.nanoen.2020.104706

Received 22 February 2020; Received in revised form 10 March 2020; Accepted 11 March 2020

Available online 16 March 2020

2211-2855/© 2020 Elsevier Ltd. All rights reserved.

Here, we proposed a superfine, coaxial, aligned and three-dimensional hierarchically interlocked PVDF/ZnO nanofibers by epitaxial growing ZnO NRs on the surface of electrospun PVDF nanofibers. The integration of high electrical performance and excellent flexibility was obtained, and the high gas permeability of the PVDF/ZnO nanofibers film was verified via the underwater bubble experiment. Besides, the interface interaction and working mechanism of PVDF/ZnO nanofibers were further explored. Furthermore, benefiting from conformal contact between PME and human skin, human vital physiological signals including respiration, wrist pulse, muscle behavior, were successfully monitored, which have anticipation to the disease rehabilitation, gait recognition and quantify muscle activity (Fig. 1a).

2. Results and discussion

The schematic fabrication process of the three-dimensional hierarchically interlocked PVDF/ZnO nanofibers was illustrated in Fig. 1b. Firstly, the high-quality oriented PVDF nanofibers were prepared by electrospinning, which presented excellent flexibility (Figs. S1 and S2a, Supporting Information). Secondly, the ZnO nanocrystal nucleation sites were conformally coated on the PVDF nanofibers fabricated by magnetron sputtering (Fig. S2b, Supporting Information), which can effectively modify the hydrophilicity of the fibers, so that the fibers were completely in contact with the hydrothermal solution and induce the growth of ZnO NRs. Finally, the *c*-axis (0001) ZnO NRs were epitaxially and co-axially grew on the PVDF nanofibers surface by the alternatively stacked zinc cations (Zn^{2+}) and oxygen anions (O^{2-}). Then the three-dimensional hierarchically interlocked PVDF/ZnO nanofibers were obtained. This nanofibers film will present several unique advantages as follows: (i) the ultrafine hierarchical PVDF/ZnO nanofibers will endow the film excellent compatibility with human epidermal for the conformal contact; (ii) the existing small gaps among nanofibers will make the as-prepared film possess high gas permeability; (iii) the electrospun PVDF nanofibers will fabricate highly electroactive phase to improve electrical performance; (iv) the interlocked ZnO NRs on the coaxial PVDF/ZnO nanofibers will produce effective deformation to enhance electrical performance.

As shown in Fig. 2a, the scanning electron microscopy (SEM) images evidently present the highly oriented three-dimensional hierarchically interlocked PVDF/ZnO nanofibers with an ultrafine diameter of about 2 μm. And the hexagonal prism shaped ZnO NRs radially grew along the surface of the PVDF nanofiber (Fig. 2b). Obviously, the core-shell PVDF/ZnO nanofiber has been intelligently co-built by the ultrafine PVDF nanofiber with a diameter of about 800 nm and the ZnO NRs with the semi diameter of about 25–50 nm (the height of 600 nm). The tops of the ZnO NRs are space-separated from each other (dozens of nanometers), while the tails are tightly connected to each other. Such a radial structure is very conducive to disperse the stress. Furthermore, the homogeneity of the PVDF/ZnO nanofibers were verified via the EDS images of a single nanofiber (Fig. 2c). When the nanofibers film was attached on the pore of the previously gas-inflated balloon, lots of timely produced air bubbles under water were obviously observed as shown in Fig. 2d and Movie S1 (Supporting Information), which exhibited high gas permeability of the as-fabricated film. Besides, the more than 360 degrees-distorted nanofibers film with a typical thickness of 35 μm evidently demonstrated its excellent flexibility and softness (Fig. 2e).

Supplementary video related to this article can be found at https://doi.org/10.1016/j.nanoen.2020.104706

As illustrated in Fig. 2f–g, the interface interaction and working mechanism of PVDF/ZnO nanofibers were further explored by the X-ray diffraction technique (XRD) and Fourier transform infrared (FTIR) spectra. From XRD patterns (Fig. 2f), PVDF nanofibers have been apparently demonstrated by both the β phase with the typical diffraction peak of 20.8° and the α phase with the diffraction peaks of 18.4° and 39.2° (JCPDS 42–1650). While the hexagonal ZnO crystalline phase has been evidently confirmed by the (002), (102) and (103) planes with the typically wurtzite-structured diffraction peaks of 34.4°, 47.5° and 62.8° (JCPDS 99–0111). Furthermore, the FTIR spectra (Fig. 2g) of PVDF/ZnO nanofibers has presented the obviously enhanced electroactive β phase with a comparison of the pure PVDF nanofibers. Specifically speaking, the characteristic α phase absorption peaks should correspond to 765 cm^{-1} (CF_2 bending) and 975 cm^{-1}(CH_2 rocking), while the typical β phase absorption peaks should correspond to 840 cm^{-1} (CH_2 rocking, CF_2 stretching and skeletal C–C stretching) and 1276 cm^{-1}. The maximum β phase content of PVDF/ZnO nanofibers $F(\beta)$ can be increased from 72% to 80% compared to pure PVDF nanofibers, which

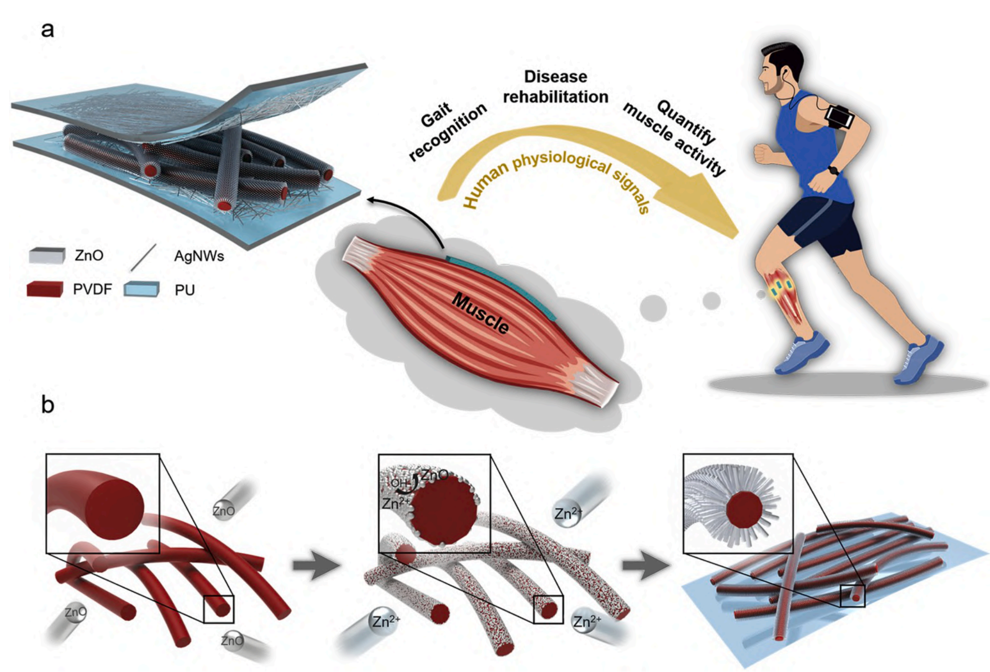

Fig. 1. The schematic diagram of the three-dimensional hierarchically interlocked PVDF/ZnO fibers-based PME for muscle behavior monitoring. (a) The PME conformally adhered to the calf muscle for the deformation monitoring. (b) The fabrication process of core-shell PVDF/ZnO nanofibers.

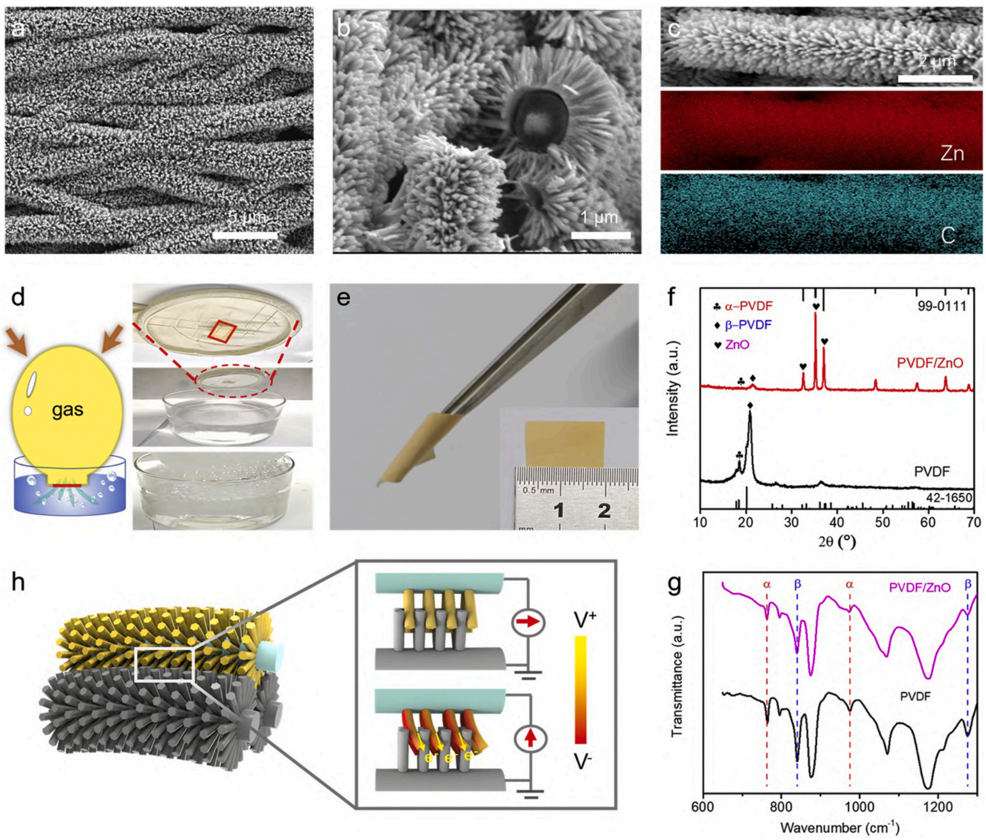

Fig. 2. The microstructure and working principle of the core-shell PVDF/ZnO nanofibers. (a) SEM image of the highly aligned PVDF/ZnO nanofibers membrane. The cross-sectional SEM image(b) and EDS mapping(c) of the PVDF/ZnO nanofiber. (d) The gas permeability test of the PVDF/ZnO nanofibers film. (e) Photograph of the highly flexible PVDF/ZnO nanofibers film. The XRD patterns(f) and FTIR spectra(g) of the PVDF and PVDF/ZnO fibers. (h) Schematic illustration of piezoelectric potential generation on the bending ZnO NRs.

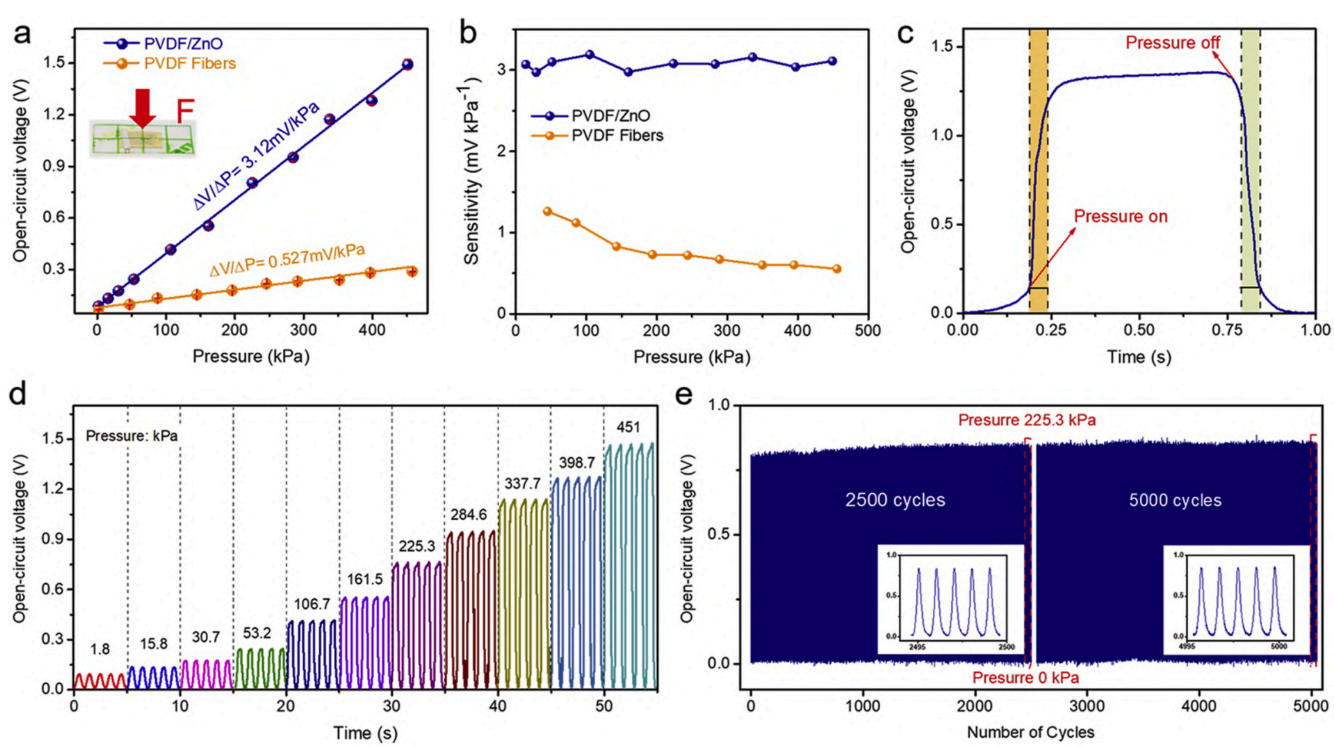

Fig. 3. Electrical and mechanical characterization of the core-shell PVDF/ZnO fibers on pressing mode. (a) Dependence of the open-circuit voltage of the device with pressure ranging from 1.8 to 451 kPa. (b) The linearity of the PME device. (c) Response time of the device on the pressure of 451 kPa. (d) The enlarged view of the open-circuit voltage under different pressures. (e) The durability test results conducted to confirm the mechanical stability of the device.

can be calculated by formula (1) [25].

$$F(\beta) = \frac{A_\beta}{\left(\frac{K_\beta}{K_\alpha}\right)A_\alpha + A_\beta} \tag{1}$$

where A_β and A_α are the absorbance at 840 cm^{-1} and 765 cm^{-1}, respectively. The K_β and K_α represent the absorption coefficients at the corresponding wavenumber, which are 6.1×10^4 cm^2 mol^{-1} and 7.7×10^4 cm^2 mol^{-1}, respectively. This improvement of the β phase content is mainly attributed to the space charge polarization at the interface of ZnO NRs and PVDF nanofibers. When growing the spontaneously polarized ZnO NRs on the PVDF surface, these gradually accumulated opposite polarity charges will also induce more β phase of PVDF nanofibers conversely (Fig. S3, Supporting Information). More importantly, when the flexible PVDF/ZnO nanofibers device is stressed, the hierarchically interlocked structure of ZnO NRs will produce abundant deformation and stronger piezoelectric potential (a pair of positive and negative piezoelectric potential on the opposite sides of the greatly curved ZnO NRs, Fig. 2h). Therefore, the synergistically piezoelectric-enhanced effect of PVDF/ZnO is expected to greatly enhance its electrical properties.

To verify the electrical performance of the PME on vertically compressive force, the device was periodically applied pressure by a linear motor at a relatively low frequency of 1 Hz. As shown in Fig. 3a, the linear monotonically increased open-circuit voltage with the pressure obviously reveals the excellent sensitivity. The pressure sensitivity (S_1) is defined as $S_1 = \Delta V/\Delta P$, where ΔP is the relative change of applied pressure, and ΔV is the relative change of output voltage. The pressure sensitivity of the PME (3.12 mV kPa^{-1} by calculating the slope of the curve) is about 6 times higher than pure PVDF nanofibers. The corresponding open-circuit voltage and the short-circuit current response curves of the PME were shown in Figs. S4 and S5, respectively. Additionally, the sensitivity of the PME over an exceptionally broad pressure range from 1.8 to 451 kPa has displayed the excellent linearity (Fig. 3b). As illustrated in Fig. 3c, the faster response times T_r/T_f are clearly observed about 53/55 ms under the pressure of 451 kPa compared to the recently reported piezoelectric sensors (80 ms [39], 290 ms [40]). Moreover, the well repeatability of the PME under various pressure loading are demonstrated with the stable and continuous signals without obvious attenuation (Fig. 3d). Furthermore, the voltage amplitudes show only a slight fluctuation after 5000 cycles, evidently revealing the high mechanical stability and durability (Fig. 3e).

Besides, the periodically curving via a linear motor (1.5 Hz) was used to measure the performance of PME with bending deformation. As shown in Fig. 4a, a curving mechanical model was utilized to analyze the film integrated onto flexible polyurethanes (PU) substrates during repeatedly bending. The out-of-plane displacement (χ) can be given by $\chi = A(1+\cos(2\pi x_1/L))/2$, where A is the amplitude and L is the initial length of the device [41]. Ascribing to the smaller thickness of the nanofibers film than the PU substrate, the curvature (ω) of the device can be evaluated as $x_1 = 0$ (the center of the device), and we can obtain the result $\omega = (-4\pi\sqrt{\Delta L/L})/L$. From Fig. 4b, two segments of the open-circuit voltage linearly increased with the curvature clearly presents the well sensitivity. The bending sensitivity (S_2) of the PME is defined as $S_2 = \Delta V/\Delta\omega$, where ΔV is the relative change of output voltage and $\Delta\omega$ is the relative change of curvature. In the range of 0–0.076 mm^{-1}, the bending sensitivity is up to 16.89 V•mm, which is about 41 times higher than that of neat PVDF nanofibers (0.41 V•mm). In the range of 0.076–0.315 mm^{-1}, the bending sensitivity is 4.8 V•mm, which is still about 11-fold improvement compared to the neat PVDF

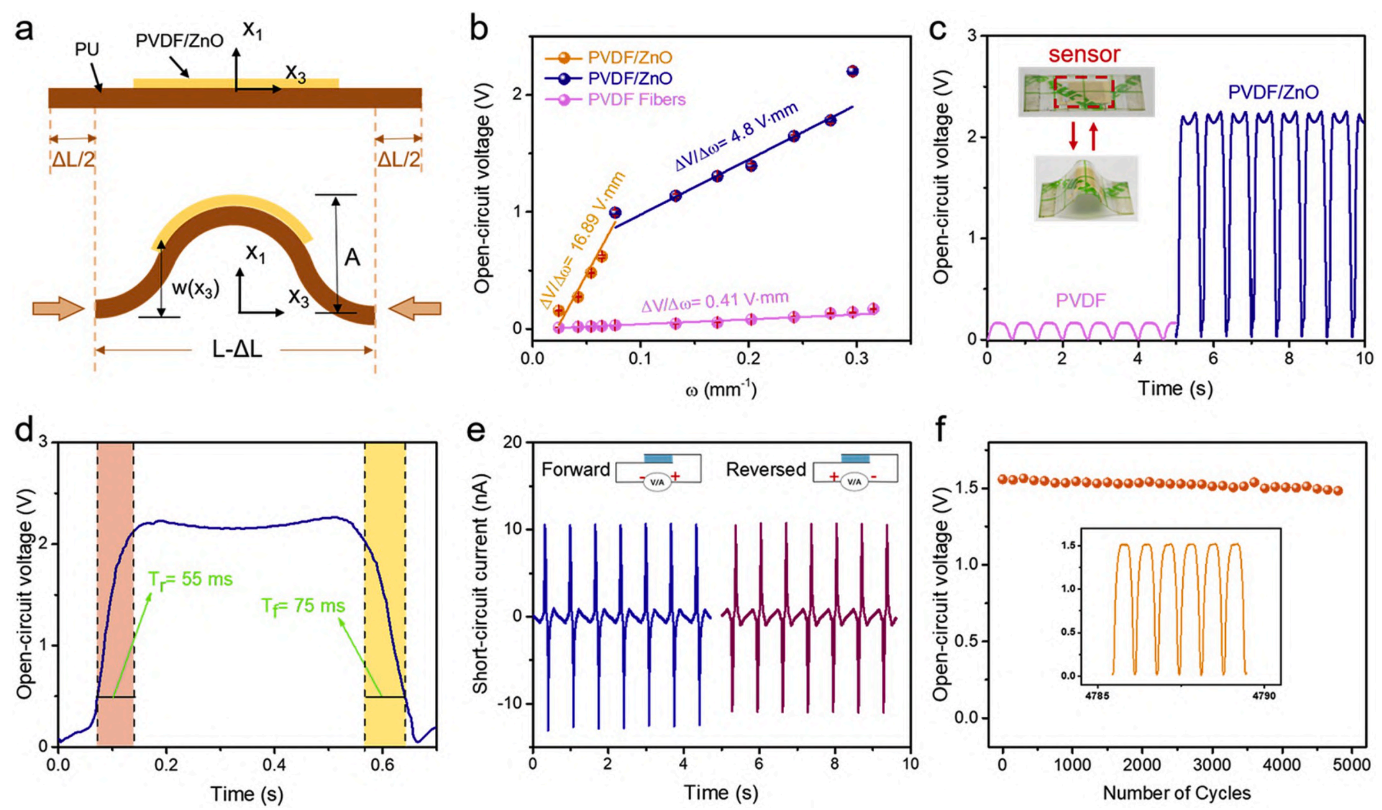

Fig. 4. Electrical and mechanical characterization of the core-shell PVDF/ZnO fibers on bending mode. (a) Schematic illustration of an analytical model for the coupling of mechanical deformation during bending. (b) Dependence of the open-circuit voltage of the device with different curvature(ω) ranging from 0.0242 mm^{-1} to 0.2962 mm^{-1}. (c) The enlarged view of the open-circuit voltage under curvature of 0.2962 mm^{-1}. (d) Response time of the device under the curvature of 0.2962 mm^{-1}. (e) Open-circuit voltage under the forward connected and reversed connected modes. (f) The durability test results conducted to confirm the mechanical stability of the device.

nanofibers. Besides, the open-circuit voltage of PVDF/ZnO nanofibers (2.23 V) is achieved while the curvature is 0.2962 mm^{-1} (Fig. 4c). And the additional details of the open-circuit voltage and short-circuit current of the device were shown in Figs. S6 and S7, respectively. Meanwhile, the quick response of the T_r/T_f times are 55/75 ms (Fig. 4d). In addition, due to the symmetrically structured nanofibers, the electrical signals purely from piezoelectric outputs can be disclosed by the identical opposite electrical outputs when the device is in forward and reverse connection (Fig. 4e). Furthermore, almost no declining of the voltage amplitudes over nearly 5000 bending cycles have demonstrated the outstanding mechanical robustness and stability of PME (Fig. 4f). The detailed curve of the output voltage is still very clear and regular at the end of the test in the magnified figure. Such excellent robustness can be attributed to the robust mechanical properties of the interlocked PVDF/ZnO core-shell nanofibers.

Owing to the above excellent electrical property, flexibility and gas permeability, along with lightweight and self-powered supply, this PME has been successfully explored for human physiological monitoring such as respiration, heart rate, and gait recognition. From Fig. 5a-I, human respiration was detected through the PME-based sensor attached on the chest. The detected breathing signals can fully comply with the realistic breathing cycles in both frequency and magnitude (Fig. 5b), and the single wave shape of the curve can correspond to a breathing cycle. These peaks and valleys are accordingly assigned to the chest expansion and shrink, respectively. These results successfully verified the ability of the PME-based sensor to clearly distinguish different breathing modes among normal breathing, deep breathing and gasping. The related video also can be found in Movie S2 (Supporting Information). The detection of human respiration not only provides effective information about cardiopulmonary function, but also can be used for alarming of sudden infant death syndrome and sleep apnea in adults. Furthermore, wrist pulse is one of the primary vital life signs to reflect heart rate, which can be used to assess the physical and health situation. As shown in Fig. 5c and Movie S3 (Supporting Information), the pulse signals can be clearly displayed owing to the PME conformally mounted on the wrist (Fig. 5a-II). From the results, the pulse frequency is about 67 beats/min,

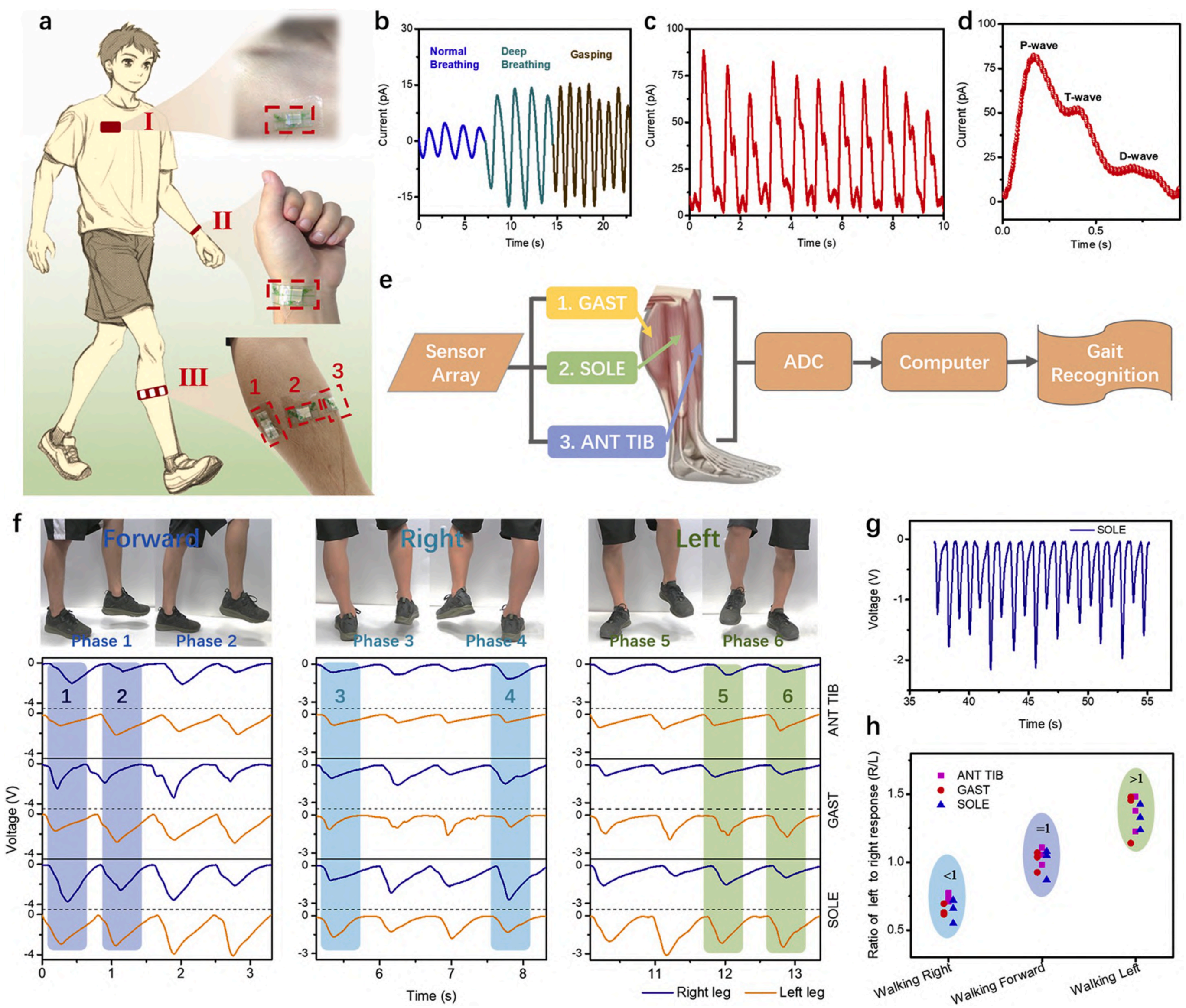

Fig. 5. Application of the flexible device for human physiological monitoring. (a) Schematic illustration of the pressure sensors assembled on chest (I), wrist (II) and three calf muscles (III). (b) The electrical outputs of different breathing patterns. (c) The real-time signals of wrist pulses of a healthy person. (d) The expanded pulse wave containing three peaks, i.e., P-wave, T-wave, D-wave. (e) Schematic diagram of the gait recognition system. (f) Signals of the ANT TIB, GAST and SOLE to detect gait states of walking forward, left and right, respectively. (g) Multiple signals of the left leg when walking left. (h) The ratio of calf response amplitude (Right leg) to the other calf response amplitude (Left leg) in different walking directions.

matching well with the normal range of a healthy person. Additionally, the percussion wave (P-wave), tidal wave (T-wave) and diastolic wave (D-wave) can be clearly distinguished in the period of a pulse, which revealed the excellent sensitivity of the designed PME-based sensors (Fig. 5d). This pulse information can be assisted in clinical applications, such as detection of hypertension, diagnosis and prevention of cardiovascular disease.

Supplementary video related to this article can be found at https://doi.org/10.1016/j.nanoen.2020.104706

Furthermore, the excellent electrical performance and well flexibility of PME arrays make them conformally and firmly adhere to the epidermis of calf muscles for the gait recognition. Fig. 5a-III shows the close attachment of three PME-based sensors on gastrocnemius (GAST), soleus (SOLE) and anterior tibias (ANT TIB) calf muscles. As shown in Fig. 5e, this gait recognition system can be realized via collecting electrical outputs of the sensors array and transferring to computer for data recording and analyzing. During walking forward, left and right, the deformation of these three muscles can be effectively detected (Fig. 5f and Movie S4). When the left foot was lifted during walking forward, a weaker voltage signals were generated on the sensors array due to the less deformation as shown in phase 1. Because the right foot is the main force-bearing foot, a stronger voltage signal was generated in this phase. The opposite voltage signals of the left and right legs will be produced during phase 2 when the right foot was lifted. Similarly, whether they are going left or right, the sensors arrays can effectively collect the correspondingly different signals as shown in phase 3–6. The well regularity and stability of walking signals was shown in Fig. 5g. In order to further contrastively analyze the output of each sensor, R can be defined as the ratio of the left to right calf electrical signal. When walking forward, the responses of three sensors attached on each leg are almost the same, so the R is close to 1. When walking left, the calf muscles on the right foot are more activated than the left foot, so the R is greater than 1. Conversely, the R will be less than 1 when walking right. Therefore, the different gait patterns can be distinguished by the different R values (Fig. 5h). Moreover, this gait recognition can helpfully analyze human walking and diagnose the Parkinson disease. Looking forward, this hierarchically structured self-powered piezoelectric sensor with well electrical performance, breathability and flexibility will render an extensive future to wearable electronics, which is of great significance to health assessment and medical science.

Supplementary video related to this article can be found at https://doi.org/10.1016/j.nanoen.2020.104706

3. Conclusions

In summary, we fabricated a unique hierarchically aligned PVDF/ZnO nanofibers with excellent flexibility, gas permeability, electrical performance, which makes a promising potential in the human physiological signals monitoring. Owing to the synergistically piezoelectric effect of the highly oriented PVDF nanofibers and the hierarchically interlocked ZnO NRs, the electrical performance has been greatly improved compared to the pure PVDF nanofibers. The pressure sensitivity (3.12 mV kPa^{-1}) of the as-fabricated sensor is nearly 6 times higher than pure PVDF and linear response over an exceptionally broad range from 1.8 to 451 kPa. The bending sensitivity (16.89 V•mm) is about 41-fold improvement compared to the neat PVDF. In addition, the PME exhibits outstanding mechanical stability over 5000 cycles on both pressing and bending modes. On this basis, the prototype of gait recognition system for the human physiological monitoring were developed, such as respiration, wrist pulse, and muscle behavior, which have great significance for healthcare assessment and illnesses diagnosis.

4. Experimental section

4.1. The preparation of PVDF nanofibers

PVDF (Kynar 720) was purchased from Arkema, and the density is 1.78 g cm^{-3}, the melt flow rate is 2.28 g min^{-1}. Firstly, PVDF (25 wt%) was added to a mixture solution (5:5 v/v) of acetone and dimethylacetamide (DMAC). Then the uniform transparent solution was obtained after magnetic stirring for 2 h in a 60 °C oil bath and pour into syringe for electrospinning. The applied high voltage is 17 kV and the flowrate is 0.03 ml min^{-1}. The speed of roller for collecting fibers is 2000 rpm and the distance of the needle is 12 cm. The as-spun PVDF nanofibers films were annealed for 2 h at 140 °C.

4.2. The preparation of ZnO nanorods

Before growing ZnO NRs, the ZnO seed layer was prepared by the radio frequency magnetron sputtering. Then the ZnO NRs were grew under the nutrient solution includes 0.1 M hexamethylenetetramine (HMTA) and 0.1 M zinc nitrate ($Zn(NO_3)2{\cdot}xH_2O$) at 85 °C for 6 h [42]. The prepared films were dried at 85 °C in the oven.

4.3. The fabrication of the sensor

The Ag NWs was purchased from Aladdin Reagent Company, and dispersing in ethanol. The Ag NWs was spin-coated on the both surface of the films at a spinning rate of 1000 rpm for 20 s and drying at 80 °C for 5 min in an oven. Then the electrode was taken out with copper wire and sealed on both sides with PU tape.

4.4. Materials characteristics

The morphologies and the structure of the PVDF/ZnO nanofibers were investigated by the field emission scanning electron microscope (FESEM, JSM-7800F) equipped with energy-dispersive X-ray spectroscopy (EDS). The crystal structures of the nanofibers were determined via X-ray diffraction technique (XRD, X Pert Mpd PRO). More information about the crystal structure of the nanofibers was obtained by Fourier-transform infrared (FTIR) in the attenuated total reflectance (ATR) mode.

4.5. Measurement of electric performance

The voltage outputs of the device were recorded by Keithley-6514 system electrometer. The current outputs of the device were measured by a low-noise current preamplifier (Stanford Research SR570). And then the signals were collected and analyzed by the Data Acquisition Card (NI PCI-6221).

Declaration of competing interest

The authors declare that they have no known competing financial interests or personal relationships that could have appeared to influence the work reported in this paper.

CRediT authorship contribution statement

Tao Yang: Conceptualization, Writing - original draft. **Hong Pan:** Methodology. **Guo Tian:** Investigation, Visualization. **Binbin Zhang:** Investigation, Funding acquisition. **Da Xiong:** Validation. **Yuyu Gao:** Resources. **Cheng Yan:** Resources. **Xiang Chu:** Validation. **Ningjun Chen:** Visualization. **Shen Zhong:** Validation. **Lei Zhang:** Formal analysis. **Weili Deng:** Funding acquisition, Writing - review & editing, Conceptualization, Project administration. **Weiqing Yang:** Funding acquisition, Writing - review & editing, Project administration.

Acknowledgments

This work was financially supported by the Sichuan province Foundation for Distinguished Young Team (No. 20CXTD0106), the National Natural Science Foundation of China (No. 61801403), the Opening Project of State Key Laboratory of Polymer Materials Engineering (Sichuan University) (No. SKLPME2019-4-27) and the Miaozi Project of Sichuan province (2019015). Thanks for the help from the Analysis and Testing Center of Southwest Jiaotong University.

Appendix A. Supplementary data

Supplementary data to this article can be found online at https://doi.org/10.1016/j.nanoen.2020.104706.

References

[1] R. Zhang, M. Hummelgård, J. Örtegren, Y. Yang, H. Andersson, E. Balliu, N. Blomquist, M. Engholm, M. Olsen, Z.L. Wang, H. Olin, Sensing body motions based on charges generated on the body, Nano Energy 63 (2019) 103842, https://doi.org/10.1016/j.nanoen.2019.06.038.
[2] T. He, H. Wang, J. Wang, X. Tian, F. Wen, Q. Shi, J.S. Ho, C. Lee, Self-sustainable wearable textile nano-energy nano-system (NENS) for next-generation healthcare applications, Adv. Sci. 6 (2019) 1901437, https://doi.org/10.1002/advs.201901437.
[3] M. Zhu, Q. Shi, T. He, Z. Yi, Y. Ma, B. Yang, T. Chen, C. Lee, Self-powered and self-functional cotton sock using piezoelectric and triboelectric hybrid mechanism for healthcare and sports monitoring, ACS Nano 13 (2019) 1940–1952, https://doi.org/10.1002/advs.201901437.
[4] Z. Lin, J. Yang, X. Li, Y. Wu, W. Wei, J. Liu, J. Chen, J. Yang, Large-scale and washable smart textiles based on triboelectric nanogenerator arrays for self-powered sleeping monitoring, Adv. Funct. Mater. 28 (2018) 1704112, https://doi.org/10.1002/adfm.201704112.
[5] M. Han, H. Wang, Y. Yang, C. Liang, W. Bai, Z. Yan, H. Li, Y. Xue, X. Wang, B. Akar, H. Zhao, H. Luan, J. Lim, I. Kandela, G.A. Ameer, Y. Zhang, Y. Huang, J.A. Rogers, Three-dimensional piezoelectric polymer microsystems for vibrational energy harvesting, robotic interfaces and biomedical implants, Nat. Electron. 2 (2019) 26–35, https://doi.org/10.1038/s41928-018-0189-7.
[6] Q. Zhang, Q. Liang, Q. Liao, F. Yi, X. Zheng, M. Ma, F. Gao, Y. Zhang, Service behavior of multifunctional triboelectric nanogenerators, Adv. Mater. 29 (2017) 1606703, https://doi.org/10.1002/adma.201606703.
[7] F. Huang, H. Yu, S. Xiang, J. Xue, H. Ming, C. Tao, N. Zhang, X. Fan, Embroidering a filmsy photo-rechargeable energy fabric with wide weather adaptability, ACS Appl. Mater. Interfaces 12 (2020) 3654–3660, https://doi.org/10.1021/acsami.9b19731.
[8] Z. Chai, N. Zhang, P. Sun, Y. Huang, C. Zhao, H. Fang, X. Fan, W. Mai, Tailorable and wearable textile devices for solar energy harvesting and simultaneous storage, ACS Nano 10 (2016) 9201–9207, https://doi.org/10.1021/acsnao.6b05293.
[9] Q. Zhang, L. Li, H. Li, L. Tang, B. He, C. Li, Z. Pan, Z. Zhou, Q. Li, J. Sun, L. Wei, X. Fan, T. Zhang, Y. Yao, Ultra-endurance coaxial-fiber stretchable sensing systems fully powered by sunlight, Nano Energy 60 (2019) 267–274, https://doi.org/10.1016/j.nanoen.2019.03.049.
[10] X. Ning, X. Yu, H. Wang, R. Sun, R.E. Corman, H. Li, C.M. Lee, Y. Xue, A. Chempakasseril, Y. Yao, Z. Zhang, H. Luan, Z. Wang, W. Xia, X. Feng, R. H. Ewoldt, Y. Huang, J.A. Rogers, Mechanically active materials in three-dimensional mesostructured, Sci. Adv. 4 (2018), https://doi.org/10.1126/sciadv.aat8313 eaat8313.
[11] K. Chen, W. Gao, S. Emaminejad, D. Kiriya, H. Ota, H.Y. Nyein, K. Takei, A. Javey, Printed carbon nanotube electronics and sensor systems, Adv. Mater. 28 (2016) 4397–4414, https://doi.org/10.1002/adma.201504958.
[12] Z. Yang, Y. Pang, X.L. Han, Y. Yang, J. Ling, M. Jian, Y. Zhang, Y. Yang, T.L. Ren, Graphene textile strain sensor with negative resistance variation for human motion detection, ACS Nano 12 (2018) 9134–9141, https://doi.org/10.1021/acsnano.8b03391.
[13] X. Wang, Y. Gu, Z. Xiong, Z. Cui, T. Zhang, Silk-molded flexible, ultrasensitive, and highly stable electronic skin for monitoring human physiological signals, Adv. Mater. 26 (2014) 1336–1342, https://doi.org/10.1002/adma.201304248.
[14] X. Wang, Z. Liu, T. Zhang, Flexible sensing electronics for wearable/attachable health monitoring, Small 13 (2017) 1602790, https://doi.org/10.1002/smll.201602790.
[15] Q. Zhang, Z. Zhang, Q. Liang, F. Gao, F. Yi, M. Ma, Q. Liao, Z. Kang, Y. Zhang, Green hybrid power system based on triboelectric nanogenerator for wearable/portable electronics, Nano Energy 55 (2019) 151–163, https://doi.org/10.1016/j.nanoen.2018.10.078.
[16] Q. Zhang, Q. Liang, Z. Zhang, Z. Kang, Q. Liao, Y. Ding, M. Ma, F. Gao, X. Zhao, Y. Zhang, Electromagnetic shielding hybrid nanogenerator for health monitoring and protection, Adv. Funct. Mater. 28 (2017) 1703801, https://doi.org/10.1002/adfm.201703801.
[17] Y. Pang, K. Zhang, Z. Yang, S. Jiang, Z. Ju, Y. Li, X. Wang, D. Wang, M. Jian, Y. Zhang, R. Liang, H. Tian, Y. Yang, T.L. Ren, Epidermis microstructure inspired graphene pressure sensor with random distributed spinosum for high sensitivity and large linearity, ACS Nano 12 (2018) 2346–2354, https://doi.org/10.1021/acsnano.7b07613.
[18] Y. Gao, C. Yan, H. Huang, T. Yang, G. Tian, D. Xiong, N. Chen, X. Chu, S. Zhong, W. Deng, Y. Fang, W. Yang, Microchannel-confined MXene based flexible piezoresistive multifunctional micro-force sensor, Adv. Funct. Mater. (2020) 1909603, https://doi.org/10.1002/adfm.201909603.
[19] C.M. Boutry, L. Beker, Y. Kaizawa, C. Vassos, H. Tran, A.C. Hinckley, R. Pfattner, S. Niu, J. Li, J. Claverie, Z. Wang, J. Chang, P.M. Fox, Z. Bao, Biodegradable and flexible arterial-pulse sensor for the wireless monitoring of blood flow, Nat. Biomed. Eng. 3 (2019) 47–57, https://doi.org/10.1038/s41551-018-0336-5.
[20] C. Yan, W. Deng, L. Jin, T. Yang, Z. Wang, X. Chu, H. Su, J. Chen, W. Yang, Epidermis-inspired ultrathin 3D cellular sensor array for self-powered biomedical monitoring, ACS Appl. Mater. Interfaces 10 (2018) 41070–41075, https://doi.org/10.1021/acsami.8b14514.
[21] K. Meng, J. Chen, X. Li, Y. Wu, W. Fan, Z. Zhou, Q. He, X. Wang, X. Fan, Y. Zhang, J. Yang, Z.L. Wang, Flexible weaving constructed self-powered pressure sensor enabling continuous diagnosis of cardiovascular disease and measurement of cuffless blood pressure, Adv. Funct. Mater. 29 (2018) 1806388, https://doi.org/10.1002/adfm.201806388.
[22] C. Yan, Y. Gao, S. Zhao, S. Zhang, Y. Zhou, W. Deng, Z. Li, G. Jiang, L. Jin, G. Tian, T. Yang, X. Chu, D. Xiong, Z. Wang, Y. Li, W. Yang, J. Chen, A linear-to-rotary hybrid nanogenerator for high-performance wearable biomechanical energy harvesting, Nano Energy 67 (2020) 104235, https://doi.org/10.1016/j.nanoen.2019.104235.
[23] K.-B. Kim, W. Jang, J.Y. Cho, S.B. Woo, D.H. Jeon, J.H. Ahn, S.D. Hong, H.Y. Koo, T.H. Sung, Transparent and flexible piezoelectric sensor for detecting human movement with a boron nitride nanosheet (BNNS), Nano Energy 54 (2018) 91–98, https://doi.org/10.1016/j.nanoen.2018.09.056.
[24] W. Deng, T. Yang, L. Jin, C. Yan, H. Huang, X. Chu, Z. Wang, D. Xiong, G. Tian, Y. Gao, H. Zhang, W. Yang, Cowpea-structured PVDF/ZnO nanofibers based flexible self-powered piezoelectric bending motion sensor towards remote control of gestures, Nano Energy 55 (2019) 516–525, https://doi.org/10.1016/j.nanoen.2018.10.049.
[25] C. Lang, J. Fang, H. Shao, X. Ding, T. Lin, High-sensitivity acoustic sensors from nanofiber webs, Nat. Commun. 7 (2016) 11108, https://doi.org/10.1038/ncomms11108.
[26] Q. Zhang, Q. Liang, Q. Liao, M. Ma, F. Gao, X. Zhao, Y. Song, L. Song, X. Xun, Y. Zhang, An amphiphobic hydraulic triboelectric nanogenerator for a self-cleaning and self-charging power system, Adv. Funt. Mater. 28 (2018) 1803117, https://doi.org/10.1002/adfm.201803117.
[27] L. Persano, C. Dagdeviren, Y. Su, Y. Zhang, S. Girardo, D. Pisignano, Y. Huang, J. A. Rogers, High performance piezoelectric devices based on aligned arrays of nanofibers of poly(vinylidenefluoride-co-trifluoroethylene), Nat. Commun. 4 (2013) 1633, https://doi.org/10.1038/ncomms2639.
[28] X. Chen, X. Li, J. Shao, N. An, H. Tian, C. Wang, T. Han, L. Wang, B. Lu, High-performance piezoelectric nanogenerators with imprinted P(VDF-TrFE)/$BaTiO_3$ nanocomposite micropillars for self-powered flexible sensors, Small 13 (2017) 1604245, https://doi.org/10.1002/smll.201604245.
[29] G. Tian, W. Deng, Y. Gao, D. Xiong, C. Yan, X. He, T. Yang, L. Jin, X. Chu, H. Zhang, W. Yan, W. Yang, Rich lamellar crystal baklava-structured PZT/PVDF piezoelectric sensor toward individual table tennis training, Nano Energy 59 (2019) 574–581, https://doi.org/10.1016/j.nanoen.2019.03.013.
[30] G. Zhang, Q. Liao, M. Ma, F. Gao, Z. Zhang, Z. Kang, Y. Zhang, Uniformly assembled vanadium doped ZnO microflowers/bacterial cellulose hybrid paper for flexible piezoelectric nanogenerators and self-powered sensors, Nano Energy 52 (2018) 501–509, https://doi.org/10.1016/j.nanoen.2018.08.020.
[31] M. Lee, C.Y. Chen, S. Wang, S.N. Cha, Y.J. Park, J.M. Kim, L.J. Chou, Z.L. Wang, A hybrid piezoelectric structure for wearable nanogenerators, Adv. Mater. 24 (2012) 1759–1764, https://doi.org/10.1002/adma.201200150.
[32] L. Zhang, S. Bai, C. Su, Y. Zheng, Y. Qin, C. Xu, Z.L. Wang, A high-reliability kevlar fiber-ZnO nanowires hybrid nanogenerator and its application on self-powered UV detection, Adv. Funct. Mater. 25 (2015) 5794–5798, https://doi.org/10.1002/adfm.201502646.
[33] Y. Mao, P. Zhao, G. McConohy, H. Yang, Y. Tong, X. Wang, Sponge-like piezoelectric polymer films for scalable and integratable nanogenerators and self-powered electronic systems, Adv. Energy Mater. 4 (2014) 1301624, https://doi.org/10.1002/aenm.201301624.
[34] X.L. Chen, J.Y. Shao, N.L. An, X.M. Li, H.M. Tian, C. Xu, Y.C. Ding, Self-powered flexible pressure sensors with vertically well-aligned piezoelectric nanowire arrays for monitoring vital signs, J. Mater. Chem. C. 3 (2015) 11806–11814, https://doi.org/10.1039/C5TC02173A.
[35] J.-H. Lee, H.-J. Yoon, T.Y. Kim, M.K. Gupta, J.H. Lee, W. Seung, H. Ryu, S.-W. Kim, Micropatterned P(VDF-TrFE) film-based piezoelectric nanogenerators for highly sensitive self-powered pressure sensors, Adv. Funct. Mater. 25 (2015) 3203–3209, https://doi.org/10.1002/adfm.201500856.
[36] Y. Qin, X. Wang, Z.L. Wang, Microfibre-nanowire hybrid structure for energy scavenging, Nature 451 (2008) 809–813, https://doi.org/10.1038/nature06601.
[37] M. Choi, G. Murillo, S. Hwang, J.W. Kim, J.H. Jung, C.-Y. Chen, M. Lee, Mechanical and electrical characterization of PVDF-ZnO hybrid structure for application to nanogenerator, Nano Energy 33 (2017) 462–468, https://doi.org/10.1016/j.nanoen.2017.01.062.
[38] G.-T. Hwang, V. Annapureddy, J.H. Han, D.J. Joe, C. Baek, D.Y. Park, D.H. Kim, J. H. Park, C.K. Jeong, K.-I. Park, J.-J. Choi, D.K. Kim, J. Ryu, K.J. Lee, Self-powered wireless sensor node enabled by an aerosol-deposited PZT flexible energy harvester, Adv. Energy Mater. 6 (2016) 1600237, https://doi.org/10.1002/aenm.201600237.

[39] J. Yan, Y. Han, S. Xia, X. Wang, Y. Zhang, J. Yu, B. Ding, Polymer template synthesis of flexible $BaTiO_3$ crystal nanofibers, Adv. Funct. Mater. 29 (2019) 1907919, https://doi.org/10.1002/adfm.201907919.
[40] W. Guo, C. Tan, K. Shi, J. Li, X.X. Wang, B. Sun, X. Huang, Y.Z. Long, P. Jiang, Wireless piezoelectric devices based on electrospun PVDF/$BaTiO_3$ NW nanocomposite fibers for human motion monitoring, Nanoscale 10 (2018) 17751–17760, https://doi.org/10.1039/C8NR05292A.
[41] C. Dagdeviren, P. Joe, O.L. Tuzman, K.-I. Park, K.J. Lee, Y. Shi, Y. Huang, J. A. Rogers, Recent progress in flexible and stretchable piezoelectric devices for mechanical energy harvesting, sensing and actuation, Extreme Mech. Lett. 9 (2016) 269–281, https://doi.org/10.1016/j.eml.2016.05.015.
[42] D. Xiong, W. Deng, G. Tian, Y. Gao, X. Chu, C. Yan, L. Jin, Y. Su, W. Yan, W. Yang, A piezo-phototronic enhanced serrate-structured ZnO-based heterojunction photodetector for optical communication, Nanoscale 11 (2019) 3021–3027, https://doi.org/10.1039/C8NR09418G.

Tao Yang received his B.S. in materials science and engineering from Southwest Jiaotong University in 2017. He is currently pursuing master's degree in materials science and engineering at Southwest Jiaotong University. His research focuses on the piezoelectric materials and wearable electronics.

Hong Pan received her master's degree in material engineering from Southwest Jiaotong University in 2017. She is a Ph. D. candidate in optoelectronic science and engineering at University of Electronic Science and Technology of China. Her research focuses on the pressure sensors and gas sensors.

Guo Tian received his B.S. degree in Material Science and Engineering from Southwest Jiaotong University, PR China in 2018. He is currently pursuing master's degree at Southwest Jiaotong University. His research interest includes piezoelectric materials and functional devices.

Binbin Zhang received his B.E. from Southwest Jiaotong University in 2015. He is currently pursuing a Ph.D. degree in materials science and engineering at Southwest Jiaotong University under the guidance of Professor Weiqing Yang.

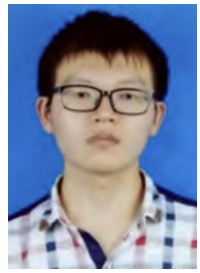

Da Xiong received his B.S. degree in Materials Science and Engineering from Southwest Jiaotong University in 2018. Now he is a doctoral candidate in Materials Scienceand Engineering at Southwest Jiaotong University. His recent research focuses on flexible optoelectronic devices and sensors.

Yuyu Gao received his B.S degree in Materials Science and Engineering from Southwest Jiaotong University,PR China in 2018. He is now a master candidate in Material Science and Engineering at Southwest Jiaotong University. His research interest includes sensitive materials and functional devices.

Cheng Yan received his B.S. from Southwest Jiaotong University in 2017. He is currently pursuing Ph.D. degree in materials science and engineering at Southwest Jiaotong University. His research focuses on the flexible electronics and self-powered sensors.

Xiang Chu received his B.S. degree in Materials Science and Engineering from Southwest Jiaotong University, PR China in 2016. He is now a doctoral candidate in Materials Science and Engineering at Southwest Jiaotong University. His research interest includes nano-materials for electrochemical energy storage devices.

Ningjun Chen received her B.S. degree in Materials Science and Engineering from Southwest Jiaotong University, PR China in 2017. She is now a doctoral candidate in Materials Science and Engineering of Southwest Jiaotong University. She specializes in two-dimensional metal carbonitrides and their energy storage mechanisms as supercapacitors.

Shen Zhong received her B.S degree in Materials Science and Engineering from Southwest Jiaotong University, PR China in 2019. She is currently pursuing master's degree in materials science and engineering at Southwest Jiaotong University. Her recent research focuses on flexible optoelectronic devices and sensors.

Lei Zhang received his B.E. degree in polymer material engineering from Chongqing University of Arts and Science in 2014. He is a graduate student in materials science and engineering at Southwest Jiaotong University under the guidance of Professor Weiqing Yang. His research focuses on the triboelectric nanogenerator and supercapacitor.

Weili Deng received his M.S. degree from Chongqing University, and Ph.D. degree in Materials Science and Engineering from Southwest Jiaotong University. He was working at the University of California, Los Angeles, as a visiting scholar from 2019 to 2020. His research interests mainly focus on piezoelectric nanomaterials and flexible electronics.

Weiqing Yang received his M.S. in Physics in 2007, and Ph.D. in Materials Science and Engineering from Sichuan University in 2011. He was a post-doctorate research fellow at University of Electronic Science and Technology of China from 2011 to 2013. Subsequently, he was a post-doctorate research fellow at Georgia Institute of Technology from 2013 to 2014, under the supervision of Prof. Zhong Lin Wang. His main research interest includes energy harvesting and storage devices, such as supercapacitors and nanogenerators.